Embedding the Sensitivities of a Structural Surrogate in a Coupled Aerostructural Wing Optimization

Joshua E. Fontana* and Pat Piperni†
Clarkson University, Potsdam, NY

Zhi Yang‡ and Dimitri J. Mavriplis§
University of Wyoming, Laramie, WY

It is well known that the most critical phases of aircraft design are the conceptual and preliminary design stages, as these have the largest impact on both the performance and economic viability of new aircraft. To this end, the work presented herein targets the preliminary design stage, in which it is imperative to have a time-efficient multidisciplinary design optimization (MDO) capability that can support evolving design requirements, whilst also facilitating interdepartmental collaboration. As the number of disciplines included in MDO processes continues to increase, it is envisioned that some of the disciplinary tools will take the form of surrogate models, while others remain physics-based, depending on the requirements and stage of the design process. To simulate this in the context of aerostructural optimization, the current work features a high-fidelity aerodynamic flow solver, while a surrogate is employed to model the wing structure. This approach includes the evaluation of the sensitivities of both the aerodynamic and structural disciplines, using a coupled-adjoint formulation to enable gradient-based optimization. An important aspect of the method is that the surrogate is trained only once, prior to the optimization, and held fixed throughout. The surrogate model in effect parameterizes the structural design process, and outputs the structural weight and equivalent stiffness of an optimized wing structure, given inputs of global geometry parameters and sizing loads. The sizing loads used to interrogate the surrogate are represented as parameterized load envelopes, which keeps the number of surrogate inputs small and allows the surrogate to be trained using a wide variety of representative load envelopes that cover the full range of the structural design space. The new method has been implemented in the Isight process integration framework, using the NSU3D Reynolds-Averaged Navier-Stokes code for the aerodynamic analysis and adjoint implementation, and a proprietary wing structure sizing code from Bombardier Aviation. In prior work, the method was applied to the aerostructural optimization of a wing in which only the weight of the structure was taken into account. In the work presented herein, the surrogate of the wing structure models both the weight and stiffness of the structure, thereby enabling the optimization of flexible wings. The method is applied to the aerostructural optimization of the CRM configuration, illustrating the effectiveness of the method.

Nomenclature

A	=	beam cross sectional area
$\bar{A}_n$	=	vector of Fourier coefficients for a parameterized lift distribution
A_n	=	concatenation of $\bar{A}_n$ and $(x/c)_{cp}$ vectors, and wing C_L
AR	=	wing aspect ratio
B	=	vector of beam parameters for sized wing structure
b	=	wing span
c	=	local chord (unless otherwise noted)

*Graduate Student, AIAA member; email: fontanj@clarkson.edu
†Associate Professor, AIAA member; email: ppiperni@clarkson.edu
‡Research Scientist, AIAA member; email: zyang@scientic-sims.com
§Professor, AIAA Associate Fellow; email: mavriplis@uwyo.edu

$C_{m,QC}$ = sectional pitching moment coefficient, about quarter-chord
C_m = sectional pitching moment coefficient
c_{av} = average chord of the wing
C_l = sectional lift coefficient
C_L = aircraft lift coefficient
C_D = aircraft drag coefficient
c_t = thrust specific fuel consumption
D = vector of all design variables (unless otherwise noted)
D_G = NSU3D geometric input parameters derived from design variables
D_0 = design variables that are shared between aerodynamic and structural disciplines, a subset of D
D_α = design variable for angle-of-attack
F_B = discrete forces derived from CFD sectional forces to be applied to beam model
F_{st} = sectional force coefficients and chords at a set of spanwise stations
F_T = total force coefficients
G = mesh deformation residuals
I_y = beam second moment of area about the out-of-plane bending axis
I_z = beam second moment of area about the in-plane bending axis
J = beam polar second moment of area
K = stiffness matrix of the beam model
L/D = lift-to-drag ratio
OBJ = objective function (unless otherwise noted)
R = flow residuals (unless otherwise noted)
Re = Reynolds Number
S = structural residuals
t/c = thickness to chord ratio at several spanwise stations
u = vector of structural state variables
u_{TB} = beam sectional twist and bending deflections
$\hat{u}_{TB}$ = sectional wing deflections used for CFD analysis
V_∞ = true airspeed
$W_{A/C}$ = aircraft maximum take-off weight
W_f = fuel weight
W_{other} = the total weight of every part of the aircraft other than the structural wing weight
W_{WS} = wing structural weight
x = mesh coordinates
x_B = coordinates of beam elastic axis for sized wing structure
$(x/c)_{cp}$ = center-of-pressure chordwise location at a given spanwise wing station
x_{sf} = wing surface coordinates from updated design variables and structural deflections
ω = vector of aerodynamic state variables
$\Delta\Lambda_{TE}$ = change in wing trailing-edge sweep at trailing-edge kink station
$\Lambda_{TE,ibk}$ = wing trailing-edge sweep inboard of trailing-edge kink station
θ = non-dimensional spanwise coordinate for the Glauert Fourier series
$(\cdot)^c$ = denotes the cruise case
$(\cdot)^s$ = denotes the sizing load case

I. Introduction

A. Background

The aerostructural optimization of aircraft wings typically involves a large number of design variables and constraints, as well as requiring advanced tools and expertise from multiple engineering disciplines. To address these challenges, the numerous approaches that have been developed over the years have focused on three general areas of development [1]: i) sensitivity analysis to enable efficient gradient-based optimization, ii) approximation modeling to mitigate long run times, and iii) problem decomposition to accommodate the organizational constraints. From the point of view of computational efficiency, it has been shown that gradient-based optimization algorithms, used in conjunction with the

coupled-adjoint technique for computing gradients, provide the greatest degree of scalability to large problems [2, 3]. However, implementing such approaches in an industrial setting can be challenging from an organizational perspective, especially as the number of disciplines considered is increased. Specialized tools are typically developed by different engineering departments, and the inherent complexity of aircraft design demands a high degree of knowledge and tool specialization. In such an environment, the identification of design responsibilities and the sharing of disciplinary tools must be done in a careful manner, to ensure their proper application at all stages of design [4]. To this end, a common and effective way to share disciplinary tools is via the intermediary of surrogate models, as these can be validated a priori by disciplinary experts and provided to end users for a target application. There is therefore a need for the development of a methodology that combines the strengths of these different approaches, i.e. that provides the computational efficiency of the coupled-adjoint method for gradient-based optimizations, while affording the disciplinary autonomy that is enabled by the use of surrogate models. To this end, a new methodology is being developed that incorporates these attributes [5]. This methodology uses a surrogate model for the structure that is integrated into a coupled-adjoint implementation for computing system derivatives.

The details and motivations of the new method, and its target application within the industrial design cycle, were presented [5]. In the current paper, the details of the coupled-adjoint formulation are developed further and the method is applied to the aerostructural optimization of a flexible wing.

II. Methodology

A. Target Design Stage

In the development of any new tool for aircraft design, it is important to identify the stage of the design process the new tool aims to benefit. It is well known that the most critical phases of design are the conceptual and preliminary design stages, as these have the largest impact on both the performance and economic viability of new aircraft. To this end, the work presented here targets the preliminary design stage, in which it is imperative to have a time-efficient multidisciplinary optimization (MDO) capability that can support evolving design requirements, whilst also facilitating interdepartmental collaboration. As the number of disciplines included in MDO processes inevitably increases, it is envisioned that some of the disciplinary tools will take the form of surrogate models, while others remain physics-based, depending on the requirements and stage of the design process. To simulate this in the context of aerostructural optimization, in the current work a high-fidelity computational fluid dynamics (CFD) solver [6] is employed for the aerodynamic analysis, while a surrogate model is used to model the wing structure. This approach also includes the evaluation of the coupled sensitivities of the aerodynamic and structural disciplines, to fully capture the interdisciplinary interactions and accelerate the convergence to an optimum design.

B. Description of New MDO Methodology

The MDO architecture developed for this research is a monolithic architecture, but is distinct from earlier architectures in that it uses a surrogate model for the structure embedded in a coupled-adjoint formulation. The surrogate approximates a structural sub-optimization, mapping geometry parameters and parameterized wing loads to both the weight and stiffness of an optimized wing structure. The motivation for developing such an approach is described below by highlighting its unique combination of features:

1) It uses analytical, parameterized representations of wing loads to size the wing structure at every design point, covering the entire range of anticipated loads for the problem at hand
2) The analytical representation of wing loads enables the optimization of the wing structure independently from the aerodynamic solution, which allows the generation of a set of pre-optimized structures prior to the aerostructural optimization process
3) It employs a surrogate model of the pre-optimized structures, which, among other benefits, facilitates a coupled-adjoint implementation by allowing the rapid evaluation of structural sensitivities via the finite differencing of the surrogate
4) Because the surrogate of the wing structure is generated beforehand, it enables the use of a monolithic optimization architecture, and also eliminates the large number of constraints associated with structural optimization, thus removing the need for the aggregation of constraints in the adjoint method
5) It is well suited for an industrial environment, which typically involves distinct disciplinary teams of experts, as the use of pre-generated surrogate models is a very effective way of sharing disciplinary tools

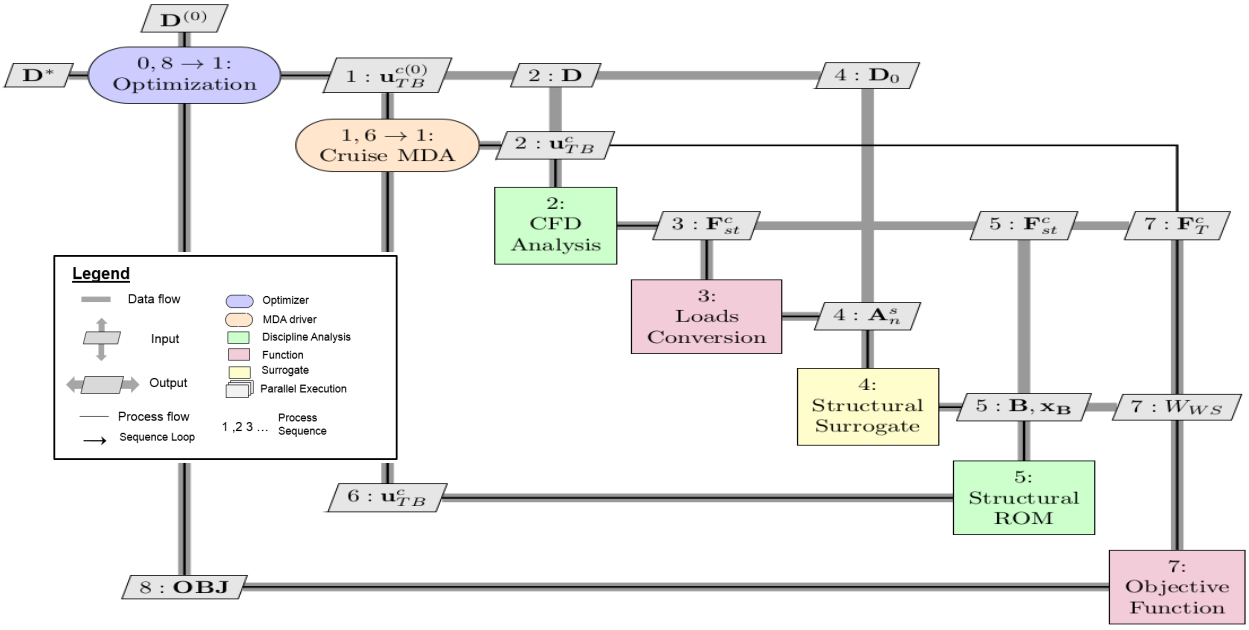

Figure 1 eXtended Design Structure Matrix (XDSM) Diagram of the MDO strategy

1. MDO Architecture

It should be noted that the optimization strategy utilized herein is a variation of the strategy proposed in previous work of the authors [5]. Like the previous architecture, it is a Multidisciplinary Feasible (MDF) [7] method that performs a multidisciplinary analysis (MDA) to converge the wing to static aeroelastic equilibrium at every design cycle, and a pre-optimized structural surrogate is employed in place of the structural analysis discipline. However, the MDO architecture described in Fontana et al.[5] features two MDA sets, one for converging the aeroelastic deformations under sizing loads, and another for converging the aeroelastic deformations under cruise loads, whereas the work presented herein is a simplified version that requires only one MDA set. This single MDA converges the aeroelastic deformations under cruise loads, while sizing the structure at every iteration by interrogating the structural surrogate model. To size the structure, the loads provided to the surrogate are the cruise loads multiplied by a scale factor to approximate a 2.5g maneuver.An eXtended Design Structure Matrix (XDSM) describing this overall process is shown in Figure 1, with its algorithm shown in Algorithm 1.

Algorithm 1: Algorithm of the New MDO Method

0: Initialize Optimization with baseline design variable values
do
  1: Initialize deflections to 0 for MDA's
  do
    2: Update mesh, based on design changes and deflections, and run CFD Solution
    3: Scale and parameterize resulting aerodynamic cruise loads according to sizing case
    4: Interrogate surrogate, using parameterized sizing loads
    5: Apply cruise loads to structural reduced-order model (ROM) output by the surrogate to obtain deflections
    6: Pass deflections to MDA driver to use for next iteration
  until *MDA has converged*;
  7: Compute objective, performing mission analysis to find fuel weight and compute total A/C weight.
  8: Pass objective value to optimizer to determine next design step
until *Optimization has converged*;

In the present work, this MDO process is carried out by means of several independent codes. The programs are executed in sequence via the SIMULIA Isight process integration framework, which also enables the automated transfer of data via file I/O. Within this framework, several of the essential functions of this setup, such as the CFD flow solution, are performed by the high-fidelity RANS solver, NSU3D [8], and its accompanying suite of programs. Specifically, the fluid-structure interface (FSI), mesh deformation tool, and flow-solution post-processor, are all part of the NSU3D program, which includes a collection of fortran modules customized for the present work. The MDO process is decomposed in detail in terms of these and the functions of other codes in Table 2. It should be noted that the NSU3D suite was chosen for this task, in part, due to its internal adjoint sensitivity capabilities [9], which are an integral part of the present method, as discussed in Section II.F.

2. Coupled-Adjoint Sensitivity Analysis

Gradient-based optimization techniques greatly reduce the expense of solving large-scale optimization problems, and thus it is desirable for any MDO method to facilitate an efficient computation of the gradients. To this end, the adjoint method provides a means of computing gradients in which the computational cost is virtually independent of the number of design variables. On the other hand, the number of objective and constraint functions do have a significant impact on the cost of the adjoint method, so ideally this number should be kept small, where possible [10, 11].

The coupled-adjoint method as described by Martins [12] forms the foundation of the adjoint implementation of the present work. However, the methodology is modified and expanded to adapt it to the new MDO strategy, and is discussed in Section II.F.

C. Loads Parameterization

1. Lift Distribution

The parameterization method chosen for the wing lift distribution is the classic Fourier series method originally developed by Glauert [13]. In this method, the lift distribution is given as

$$\frac{C_l c}{c_{av}} = 4AR \sum_n \bar{A}_n \sin(n\theta), \tag{1}$$

where c_{av} is the average chord, AR is the wing aspect ratio, and $\bar{A}_n$ are the Fourier coefficients. C_l and c are the sectional lift coefficient and the local chord, respectively, as functions of the nondimensional spanwise coordinate θ, which is defined by

$$y = (b/2)\cos(\theta), \tag{2}$$

where b is the wingspan, and y is the dimensional spanwise coordinate, ranging from $-b/2$ to $b/2$.

Further details on the expansion of equation 1 to compute the associated internal shear and bending moment distributions are provided in [5].

2. Pitching Moment Distribution

The pitching moment distribution is modeled in terms of the center-of-pressure chordwise locations at a number of wing spanwise stations. This approach is chosen because it allows the pitching moment to be linked directly to the lift distribution via the center-of-pressure location (assuming the contribution of the drag force is negligible). Therefore, the pitching moment about the quarter-chord at any spanwise station can be written as

$$C_{m,QC} = (0.25 - (x/c)_{cp})C_l, \tag{3}$$

where $(x/c)_{cp}$ is the local center-of-pressure chordwise location. To properly capture the whole spanwise pitching moment distribution, the $(x/c)_{cp}$ values are computed at a number of spanwise locations, and then interpolated with a simple piecewise polynomial function.

For convenience, the $\bar{A}_n$ and $(x/c)_{cp}$ vectors that define the lift and pitching moment distributions, respectively, and the wing C_L, are concatenated into a single vector, which is denoted as A_n:

$$A_n = (\bar{A}_n, (x/c)_{cp}, C_L) \tag{4}$$

D. Structural Surrogate

1. Inputs and Outputs

As mentioned in Section II.B.1, the structural surrogate model utilized in this work is a substitute for the disciplinary sub-optimization process, returning both the weight and equivalent stiffness of an optimized wing structure. The weight and stiffness of the sized wing structure are influenced by both geometric design variables and the sizing load. In practice, the wing loading consists of three components, namely the lift, drag and pitching moment distributions. To minimize the number of surrogate input parameters, two approximations are employed herein:

1) The drag load influence on the structure is assumed to be negligible.
2) Analytical, parameterized equations are used to model the wing load distribution.

Table 1 Surrogate Inputs and Outputs

Inputs (Geometry and Loads)	**Outputs (Stiffness and Weight)**
Load Parameters	**Beam Parameters**
C_L	x_B [3 per bay]
$\bar{A}_n$ [4 parameters]	A [1 per bay]
$(x/c)_{cp}$ [4 parameters]	I_y [1 per bay]
Geometry Parameters	I_z [1 per bay]
$b/2$	J [1 per bay]
$\Delta\Lambda_{TE}$	**Weight Parameters**
$\Lambda_{TE,ibk}$	W_{WS}
(t/c) [$\sim$ 5 variables]	
Total = $\sim$ 20 **variables**	**Total = (7*nbays) + 1 variables**

The input and output parameters of the structural model are shown in Table 1, where C_L is the total lift coefficient used to determine the first Fourier coefficient of the wing lift distribution, as discussed in the previous work [5]. $\bar{A}_n$ and $(x/c)_{cp}$ are the Fourier coefficients and spanwise center-of-pressure locations that describe the shape of the lift and pitching moment distributions, respectively, $b/2$ is the semi-span, $\Delta\Lambda_{TE}$ is the change in sweep angle of the trailing edge at the kink, $\Lambda_{TE,ibk}$ is the trailing-edge sweep inboard of the kink, and (t/c) denotes the wing maximum thickness at several wing spanwise stations. The wing maximum thickness distribution is modeled with 3 to 5 spanwise variables, depending on the wing geometry. The output beam parameters, for each bay, consist of the second moment of area about the z-axis (I_z), the second moment of area about the y-axis (I_y), the polar second moment of area (J), the cross-sectional area (A), and the elastic axis coordinates (x_B), which define the location of the beam elements. These parameters assume an Euler-Bernoulli beam model.

In the method presented here, the surrogate model of the wing structure represents the optimal structure for the given values of the design parameters. This is accomplished by optimizing the wing structure independently prior to the aerostructural optimization process. This approach enables the aerostructural optimization process to be monolithic in nature, focusing solely on the design of the wing outer mold lines.

E. Objective and Analysis Functions

In order to form the sensitivity equations, the relationships between the independent and dependent variables of the system need to be defined for both the objective equation and the residual equations. The objective equation consists of a term for the total aircraft weight and a term for a CL-target penalty, with a weighting constant multiplying each,

$$OBJ \quad = \quad \beta_1 W_{A/C} + \beta_2 (C_L^c - C_{L,Target}^c)^2 \tag{5}$$

where the aircraft total weight consists of a fuel weight term and a wing structural weight term, which are updated during the optimization, and a constant weight term, which accounts for the weight of the payload and all other aircraft components:

$$W_{A/C} = W_{WS} + W_f + W_{other} \tag{6}$$

The structural weight is the weight of the sized wing structure computed via the structural surrogate model, and the fuel weight is computed via the Breguet range equation for a fixed-range mission,

$$W_f = (W_{WS} + W_{other})\exp(\frac{Rc_t}{V_\infty(C_L^c/C_D^c)} - 1) \tag{7}$$

where R is the aircraft range, V_∞ is the true airspeed, and c_t is the thrust-specific fuel consumption.

Substituting equations 6 and 7 into equation 5, yields,

$$OBJ = \beta_1 \left((W_{WS} + W_{other})\exp(\frac{Rc_t}{V_\infty(C_L^c/C_D^c)}) \right) + \beta_2 (C_L^c - C_{L,Target}^c)^2 \tag{8}$$

W_{WS}, C_L, and C_D are the variables in equation 8 that change during the optimization. Therefore, the objective may be considered a function of these variables:

$$OBJ = OBJ(W_{WS}, C_L^c, C_D^c) \tag{9}$$

For simplicity of notation, C_L and C_D are concatenated into a vector of total force coefficients for the cruise case, denoted as F_T^c. Therefore, equation 9 may be rewritten as

$$OBJ = OBJ(W_{WS}, F_T^c) \tag{10}$$

where F_T^c and W_{WS} are obtained from the flow solver and the structural surrogate, respectively. However, the flow solver and structural surrogate are coupled in the MDA solution process. Therefore, it is necessary to describe them in terms of the entire MDA system. This is described in Table 2, where each important function of a single MDA cycle is listed, showing how each process is a function of the outputs from preceding processes.

D_G is a vector of NSU3D-specific geometric input parameters that describe the wing jig design shape, and take a different form than the overall design variables used in the Isight framework, which are denoted as the vector D. D includes both wing planform and sectional shape design variables. Therefore D_G needs to be computed from D in item 1 of Table 2 before proceeding to the functions of NSU3D, items 3 through 7. The twist and bending deflections resulting from the previous MDA cycle are denoted as $\hat{u}_{TB}^c$. These are used to update the wing surface coordinates, x_{sf}^c, within NSU3D, in conjunction with the design changes obtained through D_G. Once NSU3D moves the mesh (item 4), and computes the flow solution (item 5), sectional aerodynamic force coefficients and chords, F_{st}^c, are extracted from the results, as well as the total force coefficients, F_T. The sectional results are used to compute the parameterized sizing loads, A_n^s, in item 8. For simplicity of notation, the A_n vector listed here includes not only the Fourier coefficients to represent the shape of the spanload, but the total C_L and center-of-pressure parameters as well. The next three items of Table 2, the wing structural weight, W_{WS}, beam stiffness parameters, B, and beam elastic axis coordinates, x_B, are outputs of the structural surrogate and are therefore dependent on A_n. B represents the vector of all beam stiffness parameters,

$$B = \{A, I_y, I_z, J\} \tag{11}$$

The surrogate outputs are also dependent upon several of the Isight geometric design variables listed in Table 1. These are denoted here as the vector D_0, a subset of the Isight design variables, D, that are shared by both the aerodynamic and structural disciplines. Namely, these are the wing thickness and planform variables listed among the surrogate inputs in Table 1. The beam model produced by the surrogate is subject to the sizing loads in discrete form, and then the resulting deflections are interpolated onto the set of sectional wing stations used by NSU3D, producing u_{TB} for the next iteration.

F. Coupled-Adjoint Implementation

In addition to a surrogate model of the sized wing structure, the second main feature of the present approach is that the adjoint method is used to obtain coupled sensitivities, as stated previously. A modified version of the coupled-adjoint approach, adapted to accommodate the presence of the structural surrogate, is presented herein.

Item#	Function	Description
1	$D_G(D)$	NSU3D geometric input parameters derived from Isight design variables
2	$\hat{u}^c_{TB}(u^c_{TB})$	Sectional wing deflections used for CFD analysis
3	$x^c_{sf}(D_G, \hat{u}^c_{TB})$	New wing surface coordinates from updated design variables and structural deflections from the previous iteration of the MDA
4	$G^s(x^c, x^c_{sf})$	Mesh deformation residuals
5	$R^s(x^c, \omega^c, D^c_\alpha)$	Flow residuals
6	$F^s_{st}(x^c, \omega^c, D^c_\alpha)$	Sectional force coefficients at a set of spanwise stations
7	$F^c_T(x^c, \omega^c, D^c_\alpha)$	Total force coefficients
8	$A^s_n(F^c_{st}, D_o)$	Load parameterization for the station force coefficients
9	$W_{WS}(A^s_n, D_o)$	Weight of sized wing structure from the surrogate model
10	$B(A^s_n, D_o)$	Beam parameters for the sized wing structure from the surrogate model
11	$x_B(A^s_n, D_o)$	Beam elastic axis coordinates for the sized wing structure from the surrogate model
12	$F^c_B(F^c_{st}, x_B, D_o)$	Discrete forces to be applied to the beam model from CFD sectional forces
13	$S^c(K(B, x_B), u^c, F^c_B)$	Structural residuals for the beam model
14	$u^c_{TB}(\hat{u}^c_{TB}, x_B, u^c)$	Beam nodal twist and bending deflections at aerodynamic force stations

Table 2 Functions involved in the sizing MDA process

1. Tangent Formulation

Once all the relevant functions and variables have been established, the sensitivity equations may be derived. Here, these are derived in their tangent representation before proceeding to the adjoint formulation. The goal is to obtain the gradient of the objective, therefore we take the total derivative of the objective equation, Equation 10, yielding,

$$\frac{dOBJ}{dD} = \frac{\partial OBJ}{\partial W_{WS}}\frac{dW_{WS}}{dD} + \frac{\partial OBJ}{\partial F^c_T}\frac{dF^c_T}{dD} \tag{12}$$

The partial derivatives of the objective with respect to W_{WS} and F_T are computed analytically by differentiating equation 8. The total derivatives, on the other hand, are computed as part of the system of constraint equations formed from Table 2, in which resulting vectors from each of the 14 functions are considered the independent variables of the system.

Taking the total derivative of each function in Table 2 with respect to the Isight design variables, D, yields:

$$\frac{dD_G}{dD} = \frac{\partial D_G}{\partial D} \tag{13}$$

$$\frac{d\hat{u}^c_{TB}}{dD} = \frac{\partial \hat{u}^c_{TB}}{\partial u^c_{TB}}\frac{du^c_{TB}}{dD} \tag{14}$$

$$\frac{dx^c_{sf}}{dD} = \frac{\partial x^c_{sf}}{\partial D_G}\frac{dD_G}{dD} + \frac{\partial x^c_{sf}}{\partial u^c_{TB}}\frac{d\hat{u}^s_{TB}}{dD} \tag{15}$$

$$\frac{\partial G^c}{\partial x^c_{sf}}\frac{dx^c_{sf}}{dD} + \frac{\partial G^c}{\partial x^c}\frac{dx^c}{dD} = 0 \tag{16}$$

$$\frac{\partial R^c}{\partial x^c}\frac{dx^c}{dD} + \frac{\partial R^c}{\partial \omega^c}\frac{d\omega^c}{dD} + \frac{\partial R^c}{\partial D_\alpha}\frac{dD_\alpha}{dD} = 0 \tag{17}$$

$$\frac{dF^c_{st}}{dD} = \frac{\partial F^c_{st}}{\partial x^c}\frac{dx^c}{dD} + \frac{\partial F^c_{st}}{\partial \omega^c}\frac{d\omega^c}{dD} + \frac{\partial F^c_{st}}{\partial D_\alpha}\frac{dD_\alpha}{dD} \tag{18}$$

$$\frac{dF^c_T}{dD} = \frac{\partial F^c_T}{\partial x^c}\frac{dx^c}{dD} + \frac{\partial F^c_T}{\partial \omega^c}\frac{d\omega^c}{dD} + \frac{\partial F^c_T}{\partial D_\alpha}\frac{dD_\alpha}{dD} \tag{19}$$

$$\frac{dA^s_n}{dD} = \frac{\partial A^s_n}{\partial F^c_{st}}\frac{dF^c_{st}}{dD} + \frac{\partial A^s_n}{\partial D_o}\frac{dD_o}{dD} \tag{20}$$

$$\frac{dW_{WS}}{dD} = \frac{\partial W_{WS}}{\partial A^s_n}\frac{dA^s_n}{dD} + \frac{\partial W_{WS}}{\partial D_o}\frac{dD_o}{dD} \tag{21}$$

$$\frac{dB}{dD} = \frac{\partial B}{\partial A^s_n}\frac{dA^s_n}{dD} + \frac{\partial B}{\partial D_o}\frac{dD_o}{dD} \tag{22}$$

$$\frac{dx_B}{dD} = \frac{\partial x_B}{\partial A^s_n}\frac{dA^s_n}{dD} + \frac{\partial x_B}{\partial D_o}\frac{dD_o}{dD} \tag{23}$$

$$\frac{dF^c_B}{dD} = \frac{\partial F^c_B}{\partial F^c_{st}}\frac{dF^c_{st}}{dD} + \frac{\partial F^c_B}{\partial x_B}\frac{dx_B}{dD} + \frac{\partial F^c_B}{\partial D_o}\frac{\partial D_o}{\partial D} \tag{24}$$

$$\frac{\partial S^c}{\partial u^c}\frac{du^c}{dD} + \frac{\partial S^c}{\partial B}\frac{dB}{dD} + \frac{\partial S^c}{\partial x_B}\frac{dx_B}{dD} + \frac{\partial S^c}{\partial F^c_B}\frac{dF^c_B}{dD} = 0 \tag{25}$$

$$\frac{du^c_{TB}}{dD} = \frac{\partial u^c_{TB}}{\partial x_B}\frac{dx_B}{dD} + \frac{\partial u^c_{TB}}{\partial u^c}\frac{du^c}{dD} \tag{26}$$

Arranging equations 13 through 26 into a matrix system yields:

$$\begin{bmatrix}
I & 0 & 0 & 0 & 0 & 0 & 0 & 0 & 0 & 0 & 0 & 0 & 0 & 0 \\
0 & I & 0 & 0 & 0 & 0 & 0 & 0 & 0 & 0 & 0 & 0 & 0 & -I \\
-\frac{\partial x^c_{sf}}{\partial D_G} & -\frac{\partial x^c_{sf}}{\partial \hat{u}^c_{TB}} & I & 0 & 0 & 0 & 0 & 0 & 0 & 0 & 0 & 0 & 0 & 0 \\
0 & 0 & \frac{\partial G^c}{\partial x^c_{sf}} & \frac{\partial G^c}{\partial x^c} & 0 & 0 & 0 & 0 & 0 & 0 & 0 & 0 & 0 & 0 \\
0 & 0 & 0 & \frac{\partial R^c}{\partial x^c} & \frac{\partial R^c}{\partial \omega^c} & 0 & 0 & 0 & 0 & 0 & 0 & 0 & 0 & 0 \\
0 & 0 & 0 & -\frac{\partial F^c_{st}}{\partial x^c} & -\frac{\partial F^c_{st}}{\partial \omega^c} & I & 0 & 0 & 0 & 0 & 0 & 0 & 0 & 0 \\
0 & 0 & 0 & -\frac{\partial F^c_T}{\partial x^c} & -\frac{\partial F^c_T}{\partial \omega^c} & 0 & I & 0 & 0 & 0 & 0 & 0 & 0 & 0 \\
0 & 0 & 0 & 0 & 0 & -\frac{\partial A^s_n}{\partial F^c_{st}} & 0 & I & 0 & 0 & 0 & 0 & 0 & 0 \\
0 & 0 & 0 & 0 & 0 & 0 & 0 & -\frac{\partial W_{WS}}{\partial A^s_n} & I & 0 & 0 & 0 & 0 & 0 \\
0 & 0 & 0 & 0 & 0 & 0 & 0 & -\frac{\partial B}{\partial A^s_n} & 0 & I & 0 & 0 & 0 & 0 \\
0 & 0 & 0 & 0 & 0 & 0 & 0 & -\frac{\partial x_B}{\partial A^s_n} & 0 & 0 & I & 0 & 0 & 0 \\
0 & 0 & 0 & 0 & 0 & -\frac{\partial F^c_B}{\partial F^c_{st}} & 0 & 0 & 0 & 0 & -\frac{\partial F^c_B}{\partial x_B} & I & 0 & 0 \\
0 & 0 & 0 & 0 & 0 & 0 & 0 & 0 & 0 & \frac{\partial S^c}{\partial B} & \frac{\partial S^c}{\partial x_B} & \frac{\partial S^c}{\partial F^c_B} & \frac{\partial S^c}{\partial u^c} & 0 \\
0 & 0 & 0 & 0 & 0 & 0 & 0 & 0 & 0 & 0 & \frac{\partial u^c_{TB}}{\partial x_B} & 0 & \frac{\partial u^c_{TB}}{\partial u^c} & I
\end{bmatrix}
\begin{bmatrix}
\frac{dD^c_G}{dD} \\ \frac{d\hat{u}^c_{TB}}{dD} \\ \frac{dx^c_{sf}}{dD} \\ \frac{dx^c}{dD} \\ \frac{d\omega^c}{dD} \\ \frac{dF^c_{st}}{dD} \\ \frac{dF^c_T}{dD} \\ \frac{dA^s_n}{dD} \\ \frac{dW_{WS}}{dD} \\ \frac{dB}{dD} \\ \frac{dx_B}{dD} \\ \frac{dF^c_B}{dD} \\ \frac{du^c}{dD} \\ \frac{du^c_{TB}}{dD}
\end{bmatrix} =
\begin{bmatrix}
\frac{\partial D_G}{\partial D} \\ 0 \\ 0 \\ 0 \\ -\frac{\partial R^s}{\partial D_\alpha}\frac{dD_\alpha}{dD} \\ \frac{\partial F^s_{st}}{\partial D_\alpha}\frac{dD_\alpha}{dD} \\ \frac{\partial F^s_T}{\partial D_\alpha}\frac{dD_\alpha}{dD} \\ \frac{\partial A^s_n}{\partial D_o}\frac{dD_o}{dD} \\ \frac{\partial W_{WS}}{\partial D_o}\frac{\partial D_o}{\partial D} \\ \frac{\partial B}{\partial D_o}\frac{\partial D_o}{\partial D} \\ \frac{\partial x_B}{\partial D_\alpha}\frac{dD_\alpha}{dD} \\ \frac{\partial F^c_B}{\partial D_o}\frac{\partial D_o}{\partial D} \\ 0 \\ 0
\end{bmatrix} \tag{27}$$

Correspondingly, the objective gradient equation, given in equation 12, may be rewritten in terms of the total derivatives of the independent variables of equations 27, yielding:

$$\frac{dOBJ}{dD} = \begin{bmatrix} 0 & 0 & 0 & 0 & 0 & 0 & \frac{\partial OBJ}{\partial F_T^c} & 0 & \frac{\partial OBJ}{\partial W_{WS}} & 0 & 0 & 0 & 0 & 0 \end{bmatrix} \begin{bmatrix} \frac{dD_G}{dD} \\ \frac{d\hat{u}_{TB}^c}{dD} \\ \frac{dx_{sf}^c}{dD} \\ \frac{dx^c}{dD} \\ \frac{d\omega^c}{dD} \\ \frac{dF_{st}^c}{dD} \\ \frac{dF_T^c}{dD} \\ \frac{dA_n^s}{dD} \\ \frac{dW_{WS}}{dD} \\ \frac{dB}{dD} \\ \frac{dx_B}{dD} \\ \frac{dF_B^c}{dD} \\ \frac{du^c}{dD} \\ \frac{du_{TB}^c}{dD} \end{bmatrix} \tag{28}$$

This tangent system may be solved iteratively as follows, where k is the iteration counter:

$$\frac{d\hat{u}_{TB}^c}{dD}^{(k)} = \frac{du_{TB}^c}{dD}^{(k-1)} \tag{29}$$

$$\frac{dx_{sf}^c}{dD}^{(k)} = \frac{\partial x_{sf}^c}{\partial D_G}\frac{dD_G}{dD} + \frac{\partial x_{sf}^c}{\partial \hat{u}_{TB}^c}\frac{d\hat{u}_{TB}^c}{dD}^{(k)} \tag{30}$$

$$\frac{\partial G^c}{\partial x^c}\frac{dx^c}{dD}^{(k)} = -\frac{\partial G^c}{\partial x_{sf}^c}\frac{dx_{sf}^c}{dD}^{(k)} \tag{31}$$

$$\frac{\partial R^c}{\partial \omega^c}\frac{d\omega^c}{dD}^{(k)} = -\frac{\partial R^c}{\partial x^c}\frac{dx^c}{dD}^{(k)} - \frac{\partial R^c}{\partial D_\alpha}\frac{dD_\alpha}{dD} \tag{32}$$

$$\frac{dF_{st}^c}{dD}^{(k)} = \frac{\partial F_{st}^c}{\partial x^c}\frac{dx^c}{dD}^{(k)} + \frac{\partial F_{st}^c}{\partial \omega^c}\frac{d\omega^c}{dD}^{(k)} + \frac{\partial F_{st}^c}{\partial D_\alpha}\frac{dD_\alpha}{dD} \tag{33}$$

$$\frac{dF_T^c}{dD}^{(k)} = \frac{\partial F_T^c}{\partial x^c}\frac{dx^c}{dD}^{(k)} + \frac{\partial F_T^c}{\partial \omega^c}\frac{d\omega^c}{dD}^{(k)} + \frac{\partial F_T^c}{\partial D_\alpha}\frac{dD_\alpha}{dD} \tag{34}$$

Next, NSU3D outputs the $\frac{dF_{st}^c}{dD}^{(k)}$ matrix, as well as the $\frac{dF_T^c}{dD}^{(k)}$ matrix, and then the following equations are solved outside of NSU3D:

$$\frac{dA_n^s}{dD}^{(k)} = \frac{\partial A_n^s}{\partial F_{st}^c}\frac{dF_{st}}{dD}^{(k)} + \frac{\partial A_n^s}{\partial D_o}\frac{dD_o}{dD} \tag{35}$$

$$\frac{dW_{WS}}{dD}^{(k)} = \frac{\partial W_{WS}}{\partial A_n^s}\frac{dA_n^s}{dD}^{(k)} + \frac{\partial W_{WS}}{\partial D_o}\frac{dD_o}{dD} \tag{36}$$

$$\frac{dB}{dD}^{(k)} = \frac{\partial B}{\partial A_n^s}\frac{dA_n^s}{dD}^{(k)} + \frac{\partial B}{\partial D_o}\frac{dD_o}{dD} \tag{37}$$

$$\frac{dx_B}{dD}^{(k)} = \frac{\partial x_B}{\partial A_n^s}\frac{dA_n^s}{dD}^{(k)} + \frac{\partial x_B}{\partial D_o}\frac{dD_o}{dD} \tag{38}$$

$$\frac{dF_B^c}{dD}^{(k)} = \frac{\partial F_B^c}{\partial F_{st}^c}\frac{dF_{st}^c}{dD}^{(k)} + \frac{\partial F_B^c}{\partial x_B^s}\frac{dx_B}{dD}^{(k)} + \frac{\partial F_B^c}{\partial D_o}\frac{\partial D_o}{\partial D} \tag{39}$$

$$\frac{\partial S^c}{\partial u^c}\frac{du^c}{dD}^{(k)} = -\frac{\partial S^c}{\partial F_B^c}\frac{dF_B^c}{dD}^{(k)} - \frac{\partial S^c}{\partial B^s}\frac{dB}{dD}^{(k)} - \frac{\partial S^c}{\partial x_B^s}\frac{dx_B}{dD}^{(k)} \tag{40}$$

$$\frac{du_{TB}^c}{dD}^{(k)} = (1-\beta_r)\frac{d\hat{u}_{TB}^c}{dD}^{(k)} + \beta_r\frac{\partial \bar{u}_{TB}^c}{\partial x_B}\frac{dx_B}{dD}^{(k)} + \beta_r\frac{\partial \bar{u}_{TB}^c}{\partial u^c}\frac{du^c}{dD}^{(k)} \tag{41}$$

Then, once the total derivatives of the independent variables are obtained from the final iteration, the objective gradient is computed from equation 28.

The Tangent method for computing sensitivities is presented here because it is more intuitive to formulate and describe than the Adjoint method, and furthermore it may be used to derive the adjoint equations. However, the tangent method itself is not used in the optimization architecture. It is only a means for describing its adjoint counterpart which is presented in section II.F.2.

2. Adjoint Formulation

The adjoint system may be formed from equations 27 and 28. The coefficient matrix of the adjoint system is the transpose of the coefficient matrix of the tangent system, and the R.H.S. of the adjoint system is the transpose of the left-multiplying matrix in the objective equation of the tangent system, 28. These manipulations are explicitly described in Chapter 4 in the original coupled-adjoint work of Martins [12] as well as in previous work by one of the authors [2, 14]. Thus, the adjoint system may be written as:

$$\begin{bmatrix}
I & 0 & \frac{\partial x_{sf}^c}{\partial D_G} & 0 & 0 & 0 & 0 & 0 & 0 & 0 & 0 & 0 & 0 & 0 \\
0 & I & -\frac{\partial x_{sf}^c}{\partial \hat{u}_{TB}^c} & 0 & 0 & 0 & 0 & 0 & 0 & 0 & 0 & 0 & 0 & 0 \\
0 & 0 & I & \frac{\partial G^c}{\partial x_{sf}^c} & 0 & 0 & 0 & 0 & 0 & 0 & 0 & 0 & 0 & 0 \\
0 & 0 & 0 & \frac{\partial G^c}{\partial x^c} & \frac{\partial R^c}{\partial x^c} & -\frac{\partial F_{st}^c}{\partial x^c} & -\frac{\partial F_T^c}{\partial x^c} & 0 & 0 & 0 & 0 & 0 & 0 & 0 \\
0 & 0 & 0 & 0 & \frac{\partial R^c}{\partial \omega^c} & -\frac{\partial F_{st}^c}{\partial \omega^c} & -\frac{\partial F_T^c}{\partial \omega^c} & 0 & 0 & 0 & 0 & 0 & 0 & 0 \\
0 & 0 & 0 & 0 & 0 & I & 0 & -\frac{\partial A_n^s}{\partial F_{st}^c} & 0 & 0 & 0 & -\frac{\partial F_B^c}{\partial F_{st}^c} & 0 & 0 \\
0 & 0 & 0 & 0 & 0 & 0 & I & 0 & 0 & 0 & 0 & 0 & 0 & 0 \\
0 & 0 & 0 & 0 & 0 & 0 & 0 & I & -\frac{\partial W_{WS}}{\partial A_n^s} & -\frac{\partial B}{\partial A_n^s} & -\frac{\partial x_B}{\partial A_n^s} & 0 & 0 & 0 \\
0 & 0 & 0 & 0 & 0 & 0 & 0 & 0 & I & 0 & 0 & 0 & 0 & 0 \\
0 & 0 & 0 & 0 & 0 & 0 & 0 & 0 & 0 & I & 0 & 0 & \frac{\partial S^c}{\partial B} & 0 \\
0 & 0 & 0 & 0 & 0 & 0 & 0 & 0 & 0 & 0 & I & -\frac{\partial F_B^c}{\partial x_B} & \frac{\partial S^c}{\partial x_B} & \frac{\partial u_{TB}^c}{\partial x_B} \\
0 & 0 & 0 & 0 & 0 & 0 & 0 & 0 & 0 & 0 & 0 & I & \frac{\partial S^c}{\partial F_B^c} & 0 \\
0 & 0 & 0 & 0 & 0 & 0 & 0 & 0 & 0 & 0 & 0 & 0 & \frac{\partial S^c}{\partial u^c} & \frac{\partial u_{TB}^c}{\partial u^c} \\
0 & -I & 0 & 0 & 0 & 0 & 0 & 0 & 0 & 0 & 0 & 0 & 0 & I
\end{bmatrix}^{*}
\begin{bmatrix}
\lambda_{DG} \\ \hat{\lambda}_{u_{TB}^c} \\ \lambda_{x_{sf}^c} \\ \lambda_{x^c} \\ \lambda_{\omega^c} \\ \lambda_{F_{st}^c} \\ \lambda_{F_T^c} \\ \lambda_{A_n^s} \\ \lambda_{W_{WS}} \\ \lambda_B \\ \lambda_{x_B} \\ \lambda_{F_B^c} \\ \lambda_{S^c} \\ \lambda_{u_{TB}^c}
\end{bmatrix}
=
\begin{bmatrix}
0 \\ 0 \\ 0 \\ 0 \\ 0 \\ 0 \\ \frac{\partial OBJ}{\partial F_T^c}^T \\ 0 \\ \frac{\partial OBJ}{\partial W_{WS}}^T \\ 0 \\ 0 \\ 0 \\ 0 \\ 0
\end{bmatrix} \tag{42}$$

*Although not shown, all submatrices of the adjoint coefficient matrix are transposed

$$\frac{dOBJ}{dD} = \begin{bmatrix} \lambda_{DG}^T & \hat{\lambda}_{u_{TB}^c}^T & \lambda_{x_{sf}^c}^T & \lambda_{x^c}^T & \lambda_{\omega^c}^T & \lambda_{F_{st}^c}^T & \lambda_{F_T^c}^T & \lambda_{A_n^s}^T & \lambda_{W_{WS}}^T & \lambda_B^T & \lambda_{x_B}^T & \lambda_{F_B^c}^T & \lambda_{S^c}^T & \lambda_{u_{TB}^c}^T \end{bmatrix} \begin{bmatrix} \frac{\partial D_G}{\partial D} \\ 0 \\ 0 \\ 0 \\ -\frac{\partial R^s}{\partial D_\alpha}\frac{dD_\alpha}{dD} \\ \frac{\partial F_{st}^s}{\partial D_\alpha}\frac{dD_\alpha}{dD} \\ \frac{\partial F_T^s}{\partial D_\alpha}\frac{dD_\alpha}{dD} \\ \frac{\partial A_n^s}{\partial D_o}\frac{dD_o}{dD} \\ \frac{\partial W_{WS}}{\partial D_o}\frac{\partial D_o}{\partial D} \\ \frac{\partial B}{\partial D_o}\frac{\partial D_o}{\partial D} \\ \frac{\partial x_B}{\partial D_\alpha}\frac{dD_o}{dD} \\ \frac{\partial F_B^s}{\partial D_o}\frac{\partial D_o}{\partial D} \\ 0 \\ 0 \end{bmatrix} \tag{43}$$

Matrix equation 42 is solved from the bottom up, using an iterative process:

$$\lambda_{u_{TB}^c}^{(k)} = \hat{\lambda}_{u_{TB}^c}^{(k-1)} \tag{44}$$

$$\frac{\partial S^c}{\partial u^c}^T \lambda_{S^c}^{(k)} = \frac{\partial u_{TB}^c}{\partial u^c}^T \lambda_{u_{TB}^c}^{(k)} \tag{45}$$

$$\lambda_{F_B^c}^{(k)} = -\frac{\partial S^c}{\partial F_B^c}^T \lambda_{S^c}^{(k)} \tag{46}$$

$$\lambda_{x_B}^{(k)} = \frac{\partial F_B^c}{\partial x_B}^T \lambda_{F_B^c}^{(k)} - \frac{\partial S^c}{\partial x_B}^T \lambda_{S^c}^{(k)} + \frac{\partial u_{TB}^c}{\partial x_B}^T \lambda_{u_{TB}^c}^{(k)} \tag{47}$$

$$\lambda_B^{(k)} = -\frac{\partial S^c}{\partial B}^T \lambda_{S^c}^{(k)} \tag{48}$$

$$\lambda_{W_{WS}}^{(k)} = \frac{\partial OBJ}{\partial W_{WS}}^T \tag{49}$$

$$\lambda_{A_n^s}^{(k)} = \frac{\partial W_{WS}}{\partial A_n^s}^T \lambda_{W_{WS}}^{(k)} + \frac{\partial B}{\partial A_n^s}^T \lambda_B^{(k)} + \frac{\partial x_B}{\partial A_n^s}^T \lambda_{x_B}^{(k)} \tag{50}$$

$$\lambda_{F_T^c}^{(k)} = \frac{\partial OBJ}{\partial F_T^c}^T \tag{51}$$

$$\lambda_{F_{st}^c}^{(k)} = \frac{\partial A_n^s}{\partial F_{st}^c}^T \lambda_{A_n^s}^{(k)} + \frac{\partial F_B^c}{\partial F_{st}^c}^T \lambda_{F_B^c}^{(k)} \tag{52}$$

Next, $\lambda_{F_{st}}^{(k)}$ and $\lambda_{F_T}^{(k)}$ are passed into NSU3D master, which computes the following:

$$\frac{\partial R^c}{\partial \omega^c}^T \lambda_{\omega^c}^{(k)} = \frac{\partial F_{st}^c}{\partial \omega^c}^T \lambda_{F_{st}^c}^{(k)} + \frac{\partial F_T^c}{\partial \omega^c}^T \lambda_{F_T^c}^{(k)} \tag{53}$$

$$\frac{\partial G^c}{\partial x^c}^T \lambda_{x^c}^{(k)} = -\frac{\partial R^c}{\partial x^c}^T \lambda_{\omega^c}^{(k)} + \frac{\partial F_{st}^c}{\partial x^c}^T \lambda_{F_{st}^c}^{(k)} + \frac{\partial F_T^c}{\partial x^c}^T \lambda_{F_T^c}^{(k)} \tag{54}$$

$$\lambda_{x_{sf}^c}^{(k)} = -\frac{\partial G^c}{\partial x_{sf}^c}^T \lambda_{x^c}^{(k)} \tag{55}$$

$$\hat{\lambda}_{u_{TB}^c}^{(k)} = \frac{\partial x_{sf}^c}{\partial \hat{u}_{TB}^c}^T \lambda_{x_{sf}^c}^{(k)} \tag{56}$$

Then $\hat{\lambda}_{u^c_{TB}}$ is output from NSU3D, to be used in Isight on the next iteration. Once the MDA is complete, the following is computed in NSU3D to obtain λ_{DG}.

$$\lambda_{DG} = \frac{\partial x^c_{sf}}{\partial D_G}^T \lambda^{(last)}_{x^c_{sf}} \tag{57}$$

Lastly, the gradient of the objective is computed from equation 43, which is decomposed in the present implementation, such that some terms are computed by NSU3D, and the rest are computed by another code in the Isight workflow:

$$\frac{dOBJ}{dD} = \lambda^T_{DG}\frac{\partial D_G}{\partial D} + \begin{bmatrix}\hat{\lambda}^T_{u^c_{TB}} & \lambda^T_{x^c_{sf}} & \lambda^T_{x^c}\end{bmatrix}\begin{bmatrix}0\\0\\0\end{bmatrix} + \underbrace{\begin{bmatrix}\lambda^T_{\omega^c} & \lambda^T_{F^c_{st}} & \lambda^T_{F^c_T}\end{bmatrix}\begin{bmatrix}-\frac{\partial R^c}{\partial D_\alpha}\\ \frac{\partial F^s_{st}}{\partial D_\alpha}\\ \frac{\partial F^g_T}{\partial D_\alpha}\end{bmatrix}}_{\text{Solve inside NSU3D Master. Let this be } \lambda^T_{D\alpha}} \frac{\partial D_\alpha}{dD}$$

$$+ \begin{bmatrix}\lambda^T_{A^s_n} & \lambda^T_{W_{WS}} & \lambda^T_B & \lambda^T_{x_B} & \lambda^T_{F^c_B} & \lambda^T_{S^c} & \lambda^T_{u^c_{TB}}\end{bmatrix}\begin{bmatrix}\frac{\partial A^s_n}{\partial D_o}\frac{dD_o}{dD}\\ \frac{\partial W_{WS}}{\partial D_o}\frac{\partial D_o}{\partial D}\\ \frac{\partial B}{\partial D_o}\frac{\partial D_o}{\partial D}\\ \frac{\partial x_B}{\partial D_g}\frac{dD_o}{dD}\\ \frac{\partial F^g_B}{\partial D_o}\frac{\partial D_o}{\partial D}\\ 0\\ 0\end{bmatrix} \tag{58}$$

G. Partial Derivative Details

In order to solve the adjoint equations, the partial derivative terms in Equations 44 through 58 must be computed. The use of a structural surrogate model facilitates this, as the partial derivatives of any surrogate output with respect to any surrogate input may be computed by finite-differencing the computationally inexpensive model. Therefore, this is the means used to compute the partial derivatives of W_{WS}, B, and x_B. Some of the other partial derivative terms are internal to the NSU3D master code, and therefore are not discussed here. The remaining partial derivatives are computed analytically, including the partial derivatives of the structural residuals, S, which are determined from the linear elastic structural model as

$$S^c = K(B, x_B)u^c - F_B \tag{59}$$

$$\frac{\partial S^c}{\partial u^c} = K \tag{60}$$

$$\frac{\partial S^c}{\partial B} = \frac{\partial K}{\partial B}u^c \tag{61}$$

$$\frac{\partial S^c}{\partial x_B} = \frac{\partial K}{\partial x_B}u^c \tag{62}$$

$$\frac{\partial S^c}{\partial F^c_B} = -I \tag{63}$$

where the derivatives $\frac{\partial K}{\partial B}$ and $\frac{\partial K}{\partial x_B}$ are computed by analytically differentiating the known stiffness matrix formulation for Euler-Bernouli beam elements.

III. Implementation

A. Aerostructural Workflow

As mentioned previously, the MDO methodology developed herein has been implemented in an Isight workflow, which is described in detail in Fontana et al. [5]. For the CFD solution, mesh movement, and solution of the adjoint

equations, the NSU3D Reynolds-Averaged Navier-Stokes code [6, 8] is used. For the wing structural sizing and analysis, a proprietary code from Bombardier Aviation, called S4Wing [15], is used, in conjunction with the OptiStruct structural solver.

B. Surrogate of Wing Structural Weight and Stiffness

Structural sizing data from S4Wing was utilized to construct a surrogate model of wing structural weight and stiffness of a sized wing structure. The training data was collected via a 2000-point Optimal Latin Hypercube(OLH) DOE, for which the input parameters presented in Table 1 were the varying factors. The surrogate itself consisted of an Elliptical Basis Function (EBF) model. This combination of OLH sampling and EBF modeling was used because these were found to be effective techniques to model the wing weight in [5]. In the present work, beam parameters were also output by the surrogate to characterize the stiffness of the structure, as shown in the outputs column of Table 1.

A 200-point cross-validation error analysis was conducted to evaluate the model's fit for the structural weight output and the 157 beam parameter outputs. The coefficient of determination, R^2, for the wing weight was 0.99971, as can be seen in the correlation plot of Figure 2. This a similar level of accuracy to the previous work [5]. The R^2 values for the beam parameter outputs varied, with a minimum of 0.8312. Further work needs to be done to improve the surrogate model's fit in this regard, but the reduced order models currently produced by the surrogate are sufficient to demonstrate the expanded coupled-adjoint methodology. Figure 3 shows a sample correlation plot for one of the beam parameters.

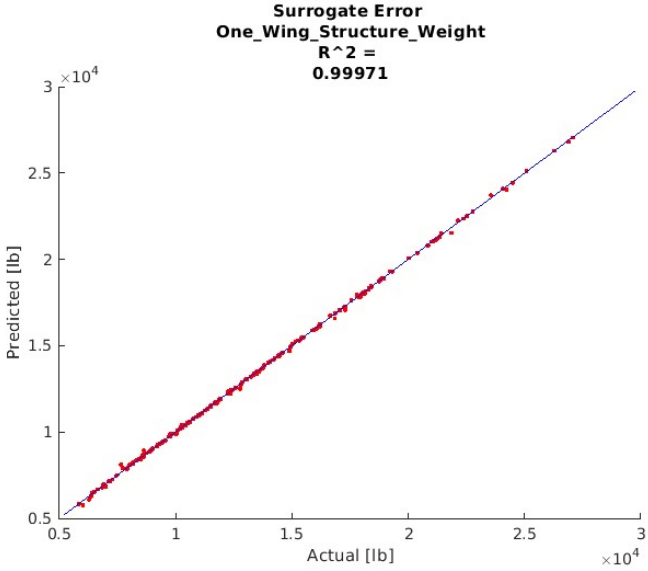

Figure 2 Cross-validation error analysis result for the surrogate wing structural weight output, W_{WS}.

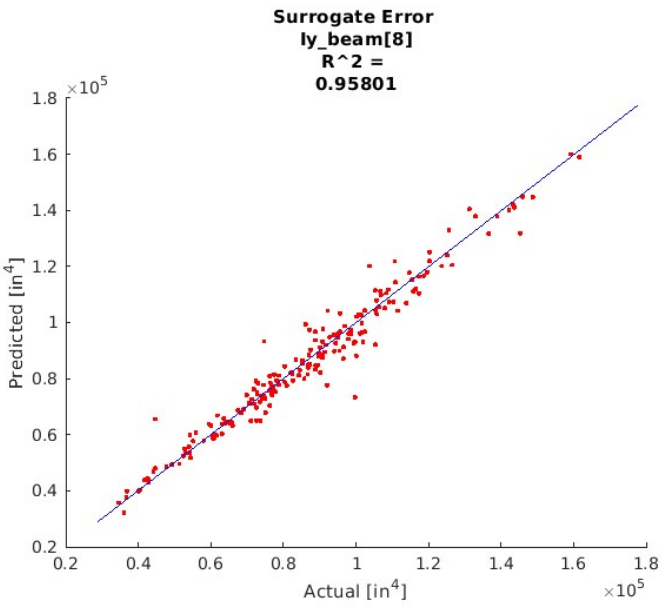

Figure 3 Sample cross-validation error analysis result for the surrogate beam parameter outputs: I_y of the 9th beam element.

IV. Results

The new methodology was applied to the aerostructural optimization of the CRM configuration. A wing-body mesh of this configuration is shown in Figure 4.

The objective of the optimization is given by equation 5. A target lift coefficient of 0.5 was enforced as part of the objective, and the gradient-based optimization algorithm used was SNOPT [16].

The values used for the weighting coefficients of the objective function, β_1 and β_2, were 0.0001 and 1000.0, respectively. The Breguet range equation (7) and equation 6 were used to compute the total aircraft weight based on the configuration L/D computed using NSU3D, and the wing structural weight, W_{WS}, obtained from the structural surrogate. The weight of the remaining components of the aircraft was based on the work of Kenway et al. [17]. For this preliminary application, the coarse mesh of the CRM wing-body configuration was used, which consists of 1.23 million nodes. To compute the lift-to-drag ratio of the configuration, 50 drag counts were added to the drag computed with this mesh, to account for the contribution from the nacelles, pylons, and tails. For the aerostructural optimization, a 2.5g maneuver load case was used to size the structure. The surrogate of the wing structure was built using the Elliptical Basis Function (EBF) technique available in the Isight process integration framework, as described in Section III.B. The standard CRM design conditions of Mach=0.85, CL=0.5, and Re= 43M were used for this optimization.

Prior to initiating the aerostructural optimization, a wing jig twist was computed for the CRM configuration, such that the original CRM flight twist was reproduced when an optimized wing structure for the CRM was subject to the 1-g cruise load case.

In the preliminary results presented here, only the wing jig twist variables and the angle of attack were activated as design variables. The results of the optimization are shown in Figures 5 to 9. As shown in Figure 5, the design objective for the aerostructural optimization converged relatively rapidly. Figure 6 shows that the optimization yielded a spanload distribution that is more loaded inboard relative to the initial spanload, which is what is expected from an aerostructural optimization. Figure 7 shows the resulting wing twist distribution, in comparison to the initial distribution. Figure 8 shows the evolution of the angle of attack required to achieve the target C_L. Figure 9 shows the evolution of the objective gradients with respect to the design variables, showing the reduction achieved in the gradients of the objective.

These preliminary results demonstrate the viability and efficiency of the new method. In particular, because the surrogate of the wing structure is held fixed, and its interrogation during the optimization is inexpensive, the new method is computationally efficient. Time and effort is required to build the surrogate prior to the optimization, however.

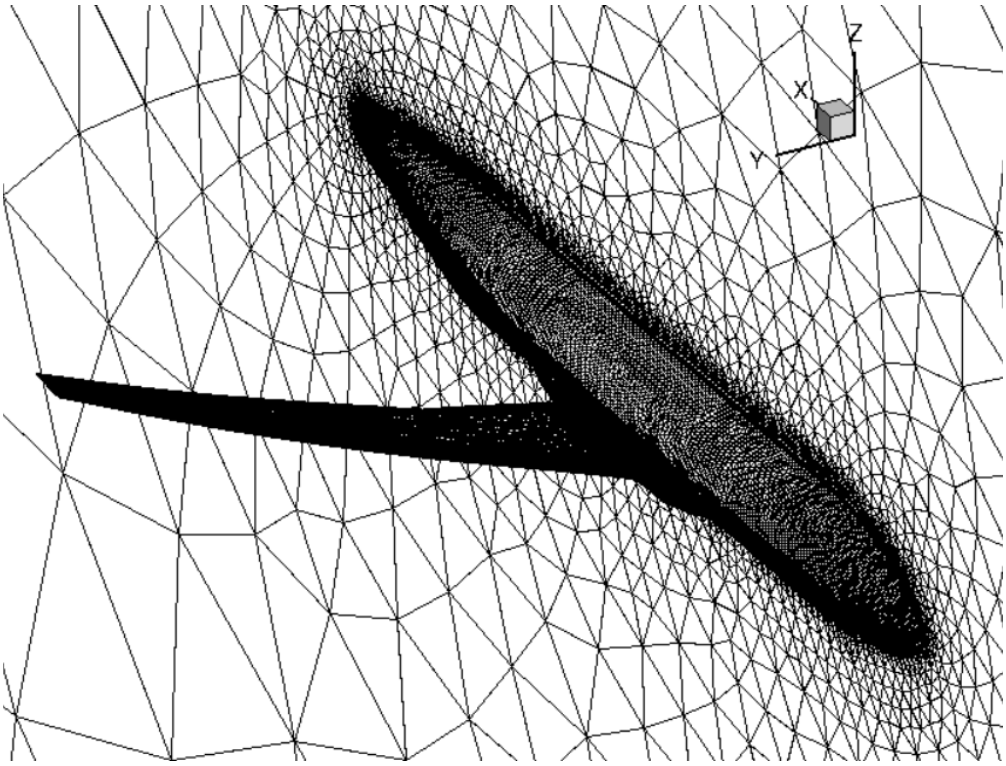

Figure 4 CRM wing-body mesh.

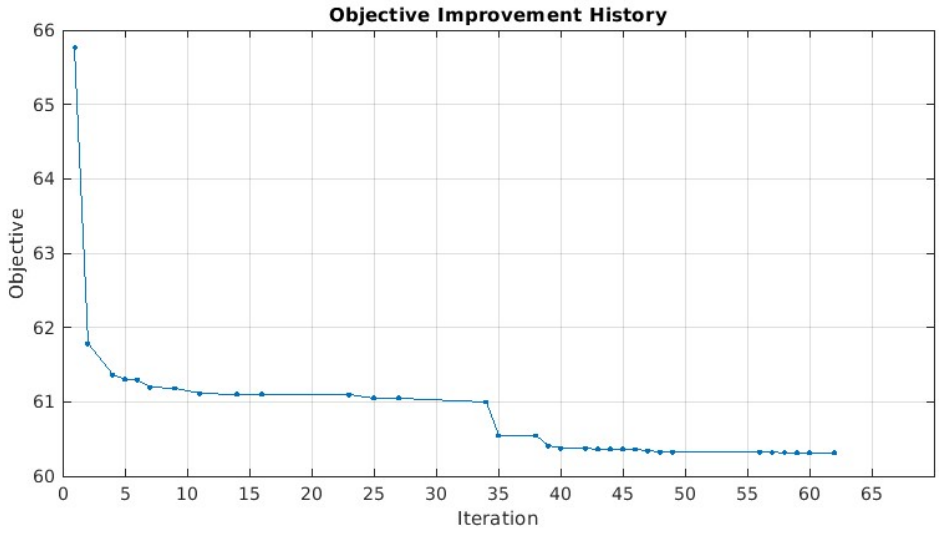

Figure 5 History of the design objective for the aerostructural optimization.

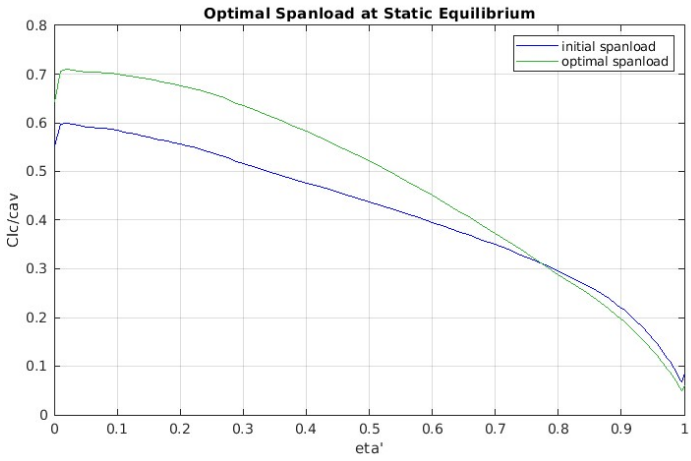

Figure 6 Wing spanload distribution resulting from the aerostructural optimization, as compared to the spanload of the initial design, both at static equilibrium.

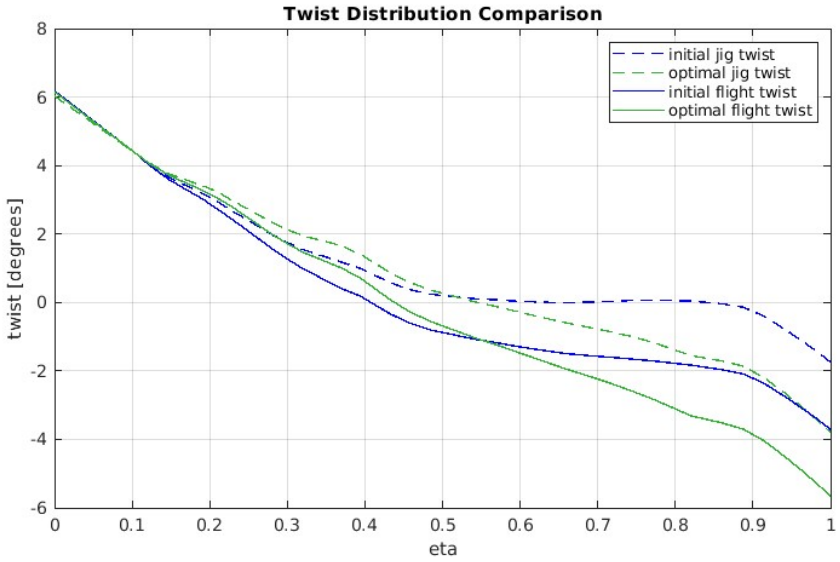

Figure 7 Twist distribution for the optimized design compared to the initial design.

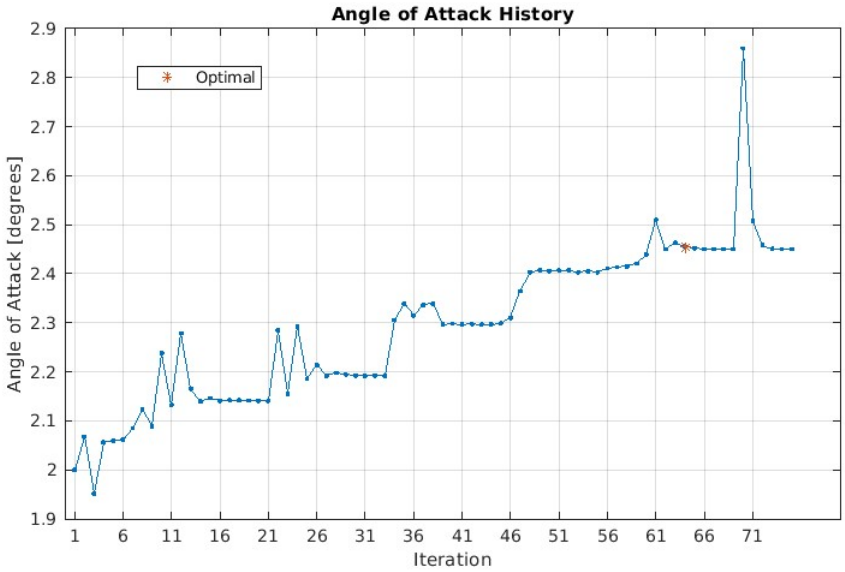

Figure 8 History of the angle-of-attack design variable.

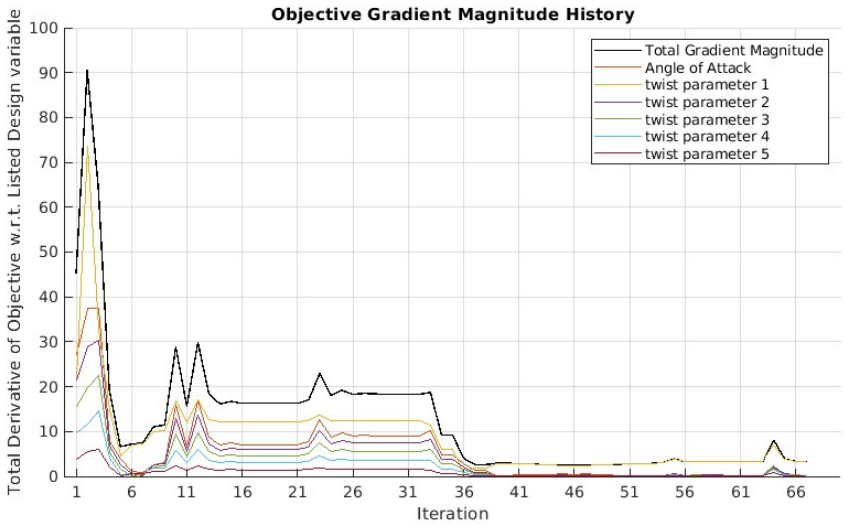

Figure 9 History of the objective gradients with respect to the design variables.

V. Conclusion

A new methodology has been developed for the aerostructural optimization of an aircraft wing at the preliminary design stage. This methodology employs a surrogate model of a pre-optimized structure, which is integrated into a coupled-adjoint formulation to enable gradient-based optimization. The new method is well suited for an industrial environment consisting of distinct disciplinary teams of experts, as the use of surrogate modeling is a very effective way of sharing tools while preserving disciplinary autonomy.

This new method has been implemented in an automated workflow using the Isight process integration software, in which the NSU3D code is used for the aerodynamic analysis, and the S4Wing and OptiStruct codes are used for the structural sizing and optimization, and building of the structural surrogate. The potential of the method has been demonstrated with preliminary results on the aerostructural optimization of the CRM wing. Future work will include

optimizations with a full set of wing design variables, including wing planform and airfoil shape parameters. In addition, two sets of MDA's will be included in the optimization, one for the cruise case and one for the sizing load case. The viability and computational efficiency of the method will be benchmarked against other methods for applications to the CRM configuration.

VI. Acknowledgments

This work was funded in part by a grant from Bombardier Aviation, Montreal, Canada. The authors are very grateful for the assistance and input provided by Denis Walch, Aerospace Structures Engineer at Bombardier Aviation. Computational resources were provided by the Advanced Research Computing Center at the University of Wyoming [18].

References

[1] Sobieszczanski-Sobieski, J., and Haftka, R. T., 'AIAA 96-0711 Multidisciplinary Aerospace Design Optimization: Survey of Recent Developments,' *34th Aerospace Sciences Meeting and Exhibit*, American Institute of Aeronautics and Astronautics, Reno, Nevada, 1995. URL https://ntrs.nasa.gov/citations/19960016674.

[2] Mavriplis, D. J., 'Discrete adjoint-based approach for optimization problems on three-dimensional unstructured meshes,' *AIAA journal*, Vol. 45, No. 4, 2007, pp. 741–750.

[3] Martins, J., and Hwang, J. T., 'Multidisciplinary Design Optimization of Aircraft Configurations—Part 1: A modular coupled-adjoint approach.' , May 2016. URL http://mdolab.engin.umich.edu, lecture series. Von Karman Institute for Fluid Dynamics, Sint-Genesius-Rode, Belgium.

[4] Piperni, P., DeBlois, A., and Henderson, R., 'Development of a Multilevel Multidisciplinary-Optimization Capability for an Industrial Environment,' *AIAA Journal*, Vol. 51, No. 10, 2013, pp. 2335–2352. doi:10.2514/1.J052180, URL https://arc.aiaa.org/doi/10.2514/1.J052180.

[5] Fontana, J. E., Piperni, P., Yang, Z., and Mavriplis, D. J., 'Coupled Aerostructural Optimization using High-Fidelity Aerodynamics and Surrogate Modeling for the Structure,' *AIAA AVIATION 2022 Forum*, American Institute of Aeronautics and Astronautics, Chicago, IL & Virtual, 2022. doi:10.2514/6.2022-3359, URL https://arc.aiaa.org/doi/10.2514/6.2022-3359.

[6] Mavriplis, D. J., Fabiano, E., and Anderson, E., 'Recent advances in high-fidelity multidisciplinary adjoint-based optimization with the NSU3D flow solver framework,' *AIAA Paper 2017-1669, 55th AIAA Aerospace Sciences Meeting*, 2017.

[7] Martins, J. R. R. A., and Lambe, A. B., 'Multidisciplinary Design Optimization: A Survey of Architectures,' *AIAA Journal*, Vol. 51, No. 9, 2013, pp. 2049–2075. doi:10.2514/1.J051895, URL http://arc.aiaa.org/doi/10.2514/1.J051895.

[8] Mavriplis, D. J., and Mani, K., 'Unstructured mesh solution techniques using the NSU3D solver,' *AIAA Paper 2014-0081, 52nd Aerospace Sciences Meeting*, 2014.

[9] Mavriplis, D. J., Fabiano, E., and Anderson, E., 'Recent Advances in High-Fidelity Multidisciplinary Adjoint-Based Optimization with the NSU3D Flow Solver Framework,' *55th AIAA Aerospace Sciences Meeting*, American Institute of Aeronautics and Astronautics, Grapevine, Texas, 2017. doi:10.2514/6.2017-1669, URL https://arc.aiaa.org/doi/10.2514/6.2017-1669.

[10] Marcelet, M., Peter, J., and Carrier, G., 'Sensitivity Analysis of a Strongly Coupled Aero-Structural System Using Direct and Adjoint Methods,' *12th AIAA/ISSMO Multidisciplinary Analysis and Optimization Conference*, American Institute of Aeronautics and Astronautics, Victoria, British Columbia, Canada, 2008. doi:10.2514/6.2008-5863, URL https://arc.aiaa.org/doi/10.2514/6.2008-5863.

[11] Fabiano, E., and Mavriplis, D., 'Adjoint-based aeroacoustic design-optimization of flexible rotors in forward flight,' *Journal of the American Helicopter Society*, Vol. 62, No. 4, 2017, pp. 1–17.

[12] Martins, J. R., 'A Coupled-Adjoint Method for High-Fidelity Aero-Structural Optimization,' PhD. dissertation, Stanford University, Dept. Aeronautics and Astronautics, Oct. 2002.

[13] Glauert, H., *The Elements of Aerofoil and Airscrew Theory*, Cambridge Universiy Press, London, UK, 1937.

[14] Mavriplis, D., 'Time Dependent Adjoint Methods for Single and Multi-disciplinary Problems,' , Sep. 2015. URL https://server.scientific-sims.com/cfdlab/scientific-sims/papers.html, 38th Advanced Computational Fluid Dynamics. Adjoint methods and their application in Computational Fluid Dynamics, VKI Lecture Series, Von Karman Institute for Fluids Dynamics, Rhode St Genese, Belgium.

[15] Walch, D., and Dervault, F., 'Convergence Strategies For Wingbox Structural Sizing Tool,' *CASI 60th Aeronautics Conference and Annual General Meeting*, Toronto, ON, Canada, 2013.

[16] Gill, P. E., Murray, W., and Saunders, M. A., 'SNOPT: An SQP Algorithm for Large-Scale Constrained Optimization,' *SIAM Journal on Optimization*, Vol. 12, No. 4, 2002, pp. 979–1006. doi:10.2307/20453604.

[17] Kenway, G., Kennedy, G., and Martins, J. R. R. A., 'Aerostructural optimization of the Common Research Model configuration,' *15th AIAA/ISSMO Multidisciplinary Analysis and Optimization Conference*, American Institute of Aeronautics and Astronautics, Atlanta, GA, 2014. doi:10.2514/6.2014-3274, URL https://arc.aiaa.org/doi/10.2514/6.2014-3274.

[18] 'Teton Computing Environment,' , 2022. Advanced Research Computing Center. University of Wyoming, https://doi.org/10.15786/M2FY47.